Sensitivity Improvement in 100 Gb/s-per-Wavelength Links Using Semiconductor Optical Amplifiers or Avalanche Photodiodes

Jose Krause Perin, Milad Sharif, and Joseph M. Kahn, *Fellow, IEEE*

***Abstract*—Intra-data-center links are scaling to 100 Gb/s per wavelength using four-level pulse-amplitude modulation (4-PAM) and direct detection, but a restrictive link budget makes it difficult to support wavelength-division multiplexing or optical circuit switching. We investigate receiver sensitivity improvements achievable using semiconductor optical amplifiers (SOAs) or avalanche photodiodes (APDs). We analyze and simulate the impact of modulator bandwidth limitations and chirp, fiber dispersion, transient SOA gain saturation, excess shot noise, and intersymbol interference caused by the APD. Using the 4-PAM and linear equalization, an SOA with 20-dB fiber-to-fiber gain and 6-dB noise figure can improve the receiver sensitivity up to 6 dB over a thermal noise-limited receiver, whereas an APD with $k_{\mathrm{A}} = 0.18$ and responsivity $R = 0.74\,\mathrm{A/W}$ provides 4.5-dB sensitivity improvement over the same reference system. We further present a simple algorithm to optimize the intensity levels and decision thresholds for a generic non-Gaussian noise distribution, which can provide an additional sensitivity improvement of 1–2 dB. For SOAs, transient gain saturation effects cause negligible sensitivity penalties, but limit the receiver dynamic range to about 15 dB for the worst case of single-wavelength pre-amplification. For APDs, we show that the APD responsivity, impact ionization factor, low-gain bandwidth, and gain-bandwidth product are all critical parameters governing the system performance.**

***Index Terms*—Communications system performance and complexity, data center interconnects, direct detection, equalization, intensity modulation, pulse amplitude modulation.**

I. Introduction

INCREASING traffic demands in data centers have motivated research on spectrally efficient modulation formats compatible with intensity modulation and direct detection (IM-DD) to replace the traditional non-return-to-zero on/off keying (NRZ-OOK) format. Recent studies for 100 Gbit/s single-laser interconnects have considered single-carrier schemes [1], such as pulse-amplitude modulation (PAM) and carrierless amplitude-and-phase (CAP), as well as multi-carrier schemes [2], such as orthogonal frequency-division multiplexing (OFDM). PAM was found to offer an attractive combination of low implementation complexity, tolerance to modulator nonlinearity, and acceptable receiver sensitivity, and four-level PAM (4-PAM) has been adopted by the IEEE P802.3bs task force [3]. An eye-safe 400 Gbit/ s link using 4-PAM with linear equalization and four wavelength-division-multiplexed (WDM) channels is expected to have an optical power margin of under 5 dB [1]. Practical systems, however, will require significantly higher margins to accommodate component aging, increased optical losses in the wavelength demultiplexer, fiber plant or optical switches, and an increased number of wavelengths, which necessitates reducing per-channel transmitted power to maintain eye safety. Thus, it is desirable to improve receiver sensitivity while minimizing system power dissipation, cost and size. Stronger forward error-correction (FEC) codes could improve sensitivity, but would dramatically increase power consumption and latency. Coherent detection could likewise improve sensitivity significantly, but it requires complex optical components and temperature-controlled lasers, while both these latter alternatives rely on costly, power-hungry digital signal processors.

Avalanche photodiodes (APD) and semiconductor amplifiers (SOA) are promising alternatives to improve receiver sensitivity. SOAs are particularly attractive because they can provide high gain over a wide bandwidth [4], circumventing the gain-bandwidth product limitations of APDs and allowing a single SOA to amplify multiple WDM channels [5]. SOAs may be realized using either bulk [6] or multiple quantum well (MQW) active layers [7]. MQW SOAs generally have higher bandwidth, gain and saturation power, and lower noise figure, but realization of polarization-independent MQW SOAs is more complicated [8].

APDs have been widely adopted in 10 Gbit/s links for metro and access networks [9], as they are more cost-effective than optical pre-amplification followed by a positive-intrinsic-negative (PIN) photodetector. 100 Gbit/s systems pose a greater challenge, however, as they require APDs with both small impact ionization factor k_A and wide bandwidth. Recent advances in APD technology have improved these characteristics. Impact ionization factors have been reduced by using a multiplication layer of InAlAs ($k_A \sim 0.2$) [10] and Si ($k_A < 0.1$) [11]. Bandwidths have been increased by new designs that decouple bandwidth from responsivity, which is normally reduced in high-speed APDs as the absorption region is made thinner to reduce transit time. These new designs include resonant cavities APDs [12], waveguide APDs [10], [13]–[15], and thin-multiplication-layer APDs in which both excess noise and avalanche buildup time are reduced by the dead zone effect [16]. Recent works

Manuscript received August 7, 2016; revised October 7, 2016; accepted October 15, 2016. Date of publication October 20, 2016; date of current version November 17, 2016. This work was supported by Maxim Integrated and by CAPES fellowship Proc. 13318/13-6. J. Krause and M. Sharif contributed equally to this work.

The authors are with the Edward L. Ginzton Laboratory, Department of Electrical Engineering, Stanford University, Stanford, CA 94305 USA (e-mail: jkperin@stanford.edu; msharif@stanford.edu; jmk@ee.stanford.edu).

Color versions of one or more of the figures in this paper are available online at http://ieeexplore.ieee.org.

Digital Object Identifier 10.1109/JLT.2016.2620139

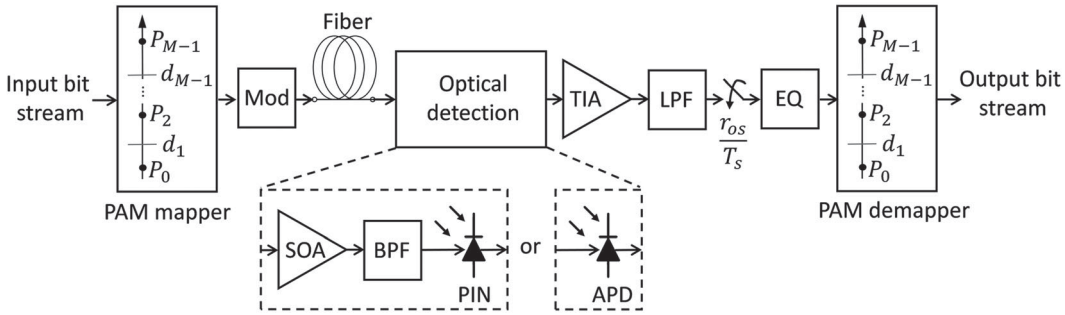

Fig. 1. System block diagram.

have also investigated using bit-synchronous sinusoidal biasing to increase the APD gain-bandwidth product (GBP) [17], [18].

This paper studies the benefits and drawbacks of SOAs and APDs in 100 Gbit/s-per-wavelength links through analysis and simulation. Previous works have studied 100 G links with SOAs through simulation [19] and experiment [20], but no work to date has presented the combination of analytical tools required for optimizing the performance of multi-level PAM systems using SOAs and APDs. Specifically, we study the combined effects of modulator bandwidth limitations and chirp, fiber CD, transient SOA gain saturation on links using an SOA for single-channel or WDM amplification and using a linear equalizer (LE) to compensate for signal distortion, and excess shot noise and inter-symbol interference caused by the APD. Moreover, we generalize the method proposed in [21], [22] to optimize intensity levels and decision thresholds for non-Gaussian signal-dependent noise, which further improves receiver sensitivity.

The remainder of this paper is organized as follows. In Section II, we present the system model used in our analyses and simulations. In Section III, we present an algorithm to optimize intensity levels and decision thresholds for non-Gaussian signal-dependent noise. In Section IV, we discuss the main component limitations and present receiver sensitivity improvement results for single-channel systems. In Section V, we present results for WDM system performance. In Section VI, we discuss important practical considerations such as temperature sensitivity and power consumption of SOA- and APD-based systems. We present conclusions in Section VII.

II. System Model

A. Intensity Modulation and Direct Detection

A general block diagram for a system using multi-level intensity modulation, optical pre-amplification and direct detection is shown in Fig. 1. At the transmitter, a stream of input bits is mapped onto *M*-PAM symbols with non-negative intensity levels $\{P_0, \ldots, P_{M-1}\}$. Digital pulse shaping can reduce the signal bandwidth and pre-compensate for the modulator frequency response, but requires a high-speed digital-to-analog converter (DAC) and, more importantly, enforcing the non-negativity of intensity modulation leads to a significant optical power penalty [1]. Hence, we assume a multi-level PAM encoder with a rectangular pulse shape. Programmable intensity levels can enable pre-compensation for modulator non-linearity and transmission of unequally spaced intensity levels to improve receiver sensitivity, as explained in Section III.

The encoder output drives an optical modulator. Both directly modulated lasers (DMLs) [23] and electro-absorption modulators (EAMs) [24] have been considered for 100 Gbit/s links. DMLs offer lower cost and power dissipation, while EAMs generally have higher bandwidth and extinction ratio. As in prior work [1], [2], we model the modulator by a critically damped second-order linear system $H_{\mathrm{mod}}(f)$ with cut-off frequency $f_{\mathrm{mod},3dB}$.

The intensity-modulated signal is launched into an SMF. The received signal after fiber propagation is detected using either an SOA-based receiver (Section II-B) or an APD-based receiver (Section II-C), as illustrated in Fig. 1. These receivers differ in three main respects: (a) The dominant noise in SOA-based receivers is signal-spontaneous beat noise, while shot-noise is the dominant noise in APD-based receivers. (b) SOAs have a wide bandwidth and do not limit the bandwidth of the receiver, in contrast to APDs, which impose significant bandwidth limitation. (c) One APD is needed for each WDM channel, whereas a single SOA can amplify multiple WDM channels.

Both systems have similar components after photo-detection: a transimpedance amplifier (TIA) followed by an equalizer. Typical TIAs have 3-dB bandwidth of 20–70 GHz and input-referred noise I_n of 20–50 $\mathrm{pA}/\sqrt{\mathrm{Hz}}$ [25], where $I_n^2 = N_0$ is the one-sided power spectrum density of thermal noise.

Due to the strong bandwidth limitations of the modulator and possibly other components such as the APD, equalization is necessary. To facilitate the analysis, we assume a symbol-rate LE with analog noise-whitening filter cascaded by an electrical filter matched to the received pulse shape. The fixed symbol-rate LE requires accurate knowledge of the channel response and precise timing recovery. In practice, a receiver employing a fixed anti-aliasing filter with an adaptive fractionally spaced LE can achieve performance approaching the ideal symbol-rate LE, while compensating for timing errors and not requiring prior knowledge of the channel.

After equalization, symbol-by-symbol detection is performed using decision thresholds $\{d_1, \ldots, d_{M-1}\}$, which may be optimized based on the statistics of the received noise, as described in Section III.

The system is assumed to use a simple Reed-Solomon code, such as the code described in [26], which has $\sim$7% overhead, provides a net coding gain of 5.6 dB and requires an input

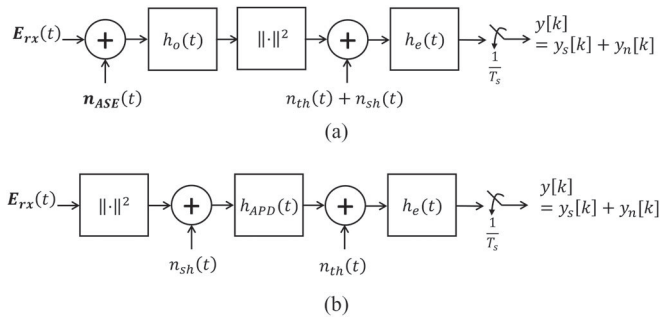

Fig. 2. Equivalent baseband block diagram for (a) SOA-based receiver and (b) APD-based receiver. Boldface variables are electric fields with two polarizations. Optical filtering is performed in each polarization independently.

bit-error ratio (BER) of 1.8×10^{-4} to achieve target output BER of 10^{-12}. In data center applications, complexity, latency, and over-clocking requirements are as important as the coding gain in FEC selection. References [26], [27] highlight FEC requirements for 100G applications.

B. Semiconductor Optical Amplifiers

In SOA-based receivers, the signal is amplified in the optical domain. Typical SOAs have fiber-to-fiber gain G as high as 30 dB [6], [7], noise figure F_n as low as 4.7 dB, and polarization-dependent gain as low as 0.2 dB [28]. At the SOA output, the amplified spontaneous emission (ASE) in each polarization can be modeled as additive white Gaussian noise (AWGN) with one-sided power spectral density (PSD)

$$S_{\mathrm{ASE}} = n_{\mathrm{sp}} (G-1) h\upsilon, \tag{1}$$

where $n_{\mathrm{sp}} \approx F_n/2$ is the spontaneous emission parameter and $h\nu$ is the photon energy.

The amplified signal passes through a band-pass optical filter to limit the ASE noise and is detected by a PIN photodetector. As the signal is assumed to be transmitted in only one polarization, a tracking polarization controller and polarizer could be used to remove the ASE polarized orthogonal to the signal prior to photo-detection. Owing to the tight power dissipation and cost budget, this polarizer is omitted from our design.

Neglecting the impact of laser intensity noise, modulator nonlinearity and chirp, fiber CD and SOA polarization-dependent gain, we describe the SOA-based receiver by its baseband equivalent model [29].

Fig. 2(a) illustrates the receiver equivalent baseband model for a pre-amplified system. $h_o(t)$ and $h_e(t)$ are the baseband equivalent transfer functions of optical filter and post-detection electrical filter, respectively. For an ideal receiver, $h_e(t)$ can be approximated by the cascade of the matched filter and the continuous-time equivalent of the LE.

For high-gain amplifiers, the total received noise is generally dominated by the beat term between the received optical signal and ASE in the same polarization. Consequently, inclusion of a polarization tracker and a polarizer to block the orthogonal ASE component would provide only a negligible performance improvement.

Owing to square-law detection, the samples of the received signal $y(t)$ are non-Gaussian. Hence, the BER must be evaluated using the conditional moment generating function (MGF) of $y[k] = y(t_k)$, which can be obtained through a Karhunen-Loéve series expansion (KLSE) of the received samples [29], [30]. Using the MGF of the samples, given the decision thresholds, error probabilities can be accurately estimated using the saddle-point approximation [31].

The signal and ASE components of $y[k]$ are described by a sum of non-central chi-square independent random variables whose MGF is

$$\Psi(s) = \prod_{n=1}^{\infty} \frac{1}{(1-\lambda_n S_{\mathrm{ASE}} s)^P} \exp\left(\frac{\lambda_n |s_n(t)|^2 s}{1-\lambda_n S_{\mathrm{ASE}} s}\right), \tag{2}$$

where and λ_n and $s_n(t)$ are obtained through the KLSE, as described in [30]; $P = 1$ or 2 depending on whether the ASE is detected in one or two polarizations.

The MGF of $y[k]$ including all noise sources in Fig. 2(a) can be calculated as a product of the MGFs for the different noises, since ASE, shot noise and thermal noise are assumed mutually independent.

Due to ISI, the statistics of $y[k]$ depends on the previous samples. In order to model this interference accurately, we model an M-PAM signal using M-ary De Bruijn sequences of order n, which comprise all possible n-symbol patterns, and we report the average BER. Unless otherwise mentioned, we use $n = 3$ in our analysis, which is sufficient to model the ISI caused by the modulator.

C. Avalanche Photodiodes

APDs provide internal electrical gain through impact ionization. This gain comes at the expense of excess shot noise due to the inherently stochastic nature of the impact ionization process. Moreover, the avalanche process increases the carrier transit time through the multiplication region, an effect known as avalanche buildup. As a result, the APD bandwidth decreases as the gain increases. This dependency is often expressed as a constraint on the GBP of the APD.

Fig. 2(b) illustrates the receiver equivalent baseband model for the APD-based receiver. The APD filters both signal and shot noise. Similarly to SOA-based system, $h_e(t)$ denotes the baseband equivalent transfer function of the post-detection electrical filter. In an ideal APD-based system, $h_e(t)$ can be approximated by the cascade of the noise whitening filter, matched filter, and the continuous-time equivalent of the LE.

Unlike a SOA-based system, shot noise is the dominant source of noise in APD-based systems. The received optical powers of interest here are high (e.g., above -16 dBm, where a thermal noise-limited, ISI-free receiver for 100 Gbit/s NRZ OOK achieves $\sim 10^{-4}$ BER, assuming an input-referred noise of 30 $\mathrm{pA}/\sqrt{\mathrm{Hz}}$). At such power levels, far from the quantum regime, shot noise can be described accurately as a white Gaussian noise whose one-sided PSD, ignoring the APD frequency

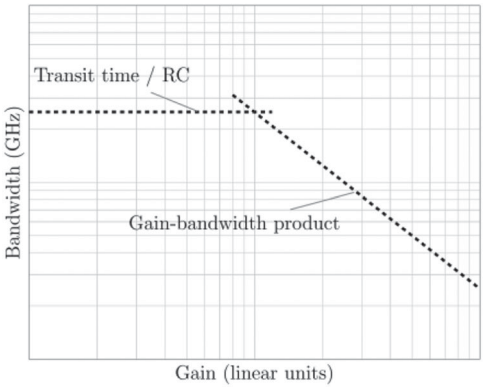

Fig. 3. Generic bandwidth-vs.-gain curve for avalanche photodiodes.

response, is given by the well-known expression

$$S_{\rm sh} = 2qG^2F_A\,(G)\,(RP_{\rm rx} + I_d)\,, \tag{3}$$

where q is the electron charge, G is the APD gain, R is the APD responsivity, $P_{\rm rx}$is the received optical power, I_d is the APD dark current and $F_A(G) = k_AG + (1 - k_A)(2 - 1/G)$ is the APD excess noise factor.

The Gaussian approximation allows us to calculate the BER without relying on MGFs and the saddle point approximation, but it must be used with caution. As shown in [34], the Gaussian approximation can be inadequate for evaluating receiver performance when ISI is introduced by an APD in the avalanche buildup time-limited regime. In this work, however, the modulator and APD (and possibly fiber propagation) all cause considerable ISI. Moreover, as discussed in Section IV-B, there is only a small sensitivity penalty for operating the APD at relatively small gains, such that the deterministic transit time and RC time constant limit the bandwidth more than avalanche buildup. Hence, the Gaussian approximation is sufficiently accurate to predict the performance at the relatively high BERs ($\sim 10^{-4}$) at which coded systems can operate.

Nevertheless, equation (3) does not account for the APD frequency response, which filters both signal and shot noise. Exact computation of the filtered shot noise variance at the APD output would require knowledge of the second-order statistics of the impulse response, which is generally not tractable analytically and requires computationally intensive simulations [33], [34]. To circumvent this problem, simpler models, such as parametric or deterministic impulse response functions, are customarily employed [35]. In this work, we model the impulse response of the APD by a deterministic exponential decay, which results in a frequency response

$$H_{\rm APD}\,(f) = \left(1 + j\frac{f}{B(G)}\right)^{-1}, \tag{4}$$

where $B(G)$ is the 3-dB bandwidth of the APD at gain G. Operating regimes for this model are illustrated in Fig. 3. At low gains, the bandwidth is generally independent of gain, since in this regime the major bandwidth limitation comes from carrier transit time and parasitic capacitance (RC time constant). As the gain increases, avalanche buildup time dominates, leading to a fixed GBP. In this model, an APD frequency response can be characterized by its low-gain bandwidth and by its GBP. Table I shows typical values of these parameters for state-of-the-art APDs.

The choice of a deterministic exponential decay for the impulse response is consistent with the transit-time/RC limited regime, but it does not capture the intrinsic correlation between an APD's gain and its impulse response. As shown in [35], however, this problem can be mitigated by using a shot noise equivalent bandwidth, as opposed to the APD's 3-dB bandwidth, in computing the shot noise variance. This definition of noise bandwidth approximately captures the fluctuations in the impulse response as well as in the gain, and may exceed an APD's 3-dB bandwidth by up to 30% [35]. This definition also captures the effect of dead space in APDs. Dead space is the distance a newly generated carrier must propagate before gaining sufficient energy to impact ionize other carriers. This effect is particularly important in thin APDs [16].

III. Optimization of Intensity Levels and Decision Thresholds

As discussed in Sections II-B and II-C, signal-spontaneous beat noise is the dominant noise in pre-amplified systems, whereas shot noise is the dominant noise for APD-based systems. In either case, the dominant noise is signal dependent and hence we can improve receiver sensitivity by properly setting the intensity levels and decision thresholds.

Our objective is to minimize the average optical power required to achieve a given average error probability. The approach adopted here is to sequentially adjust the levels $\{P_0, P_1, \ldots, P_{M-1}\}$ and decision thresholds $\{d_1, d_2, \ldots, d_{M-1}\}$ to obtain an error probability $P_{\rm e}$ that is equal at all $M-1$ thresholds, considering upward and downward errors. Specifically, for intensity level $P_{\rm i}$, we set the decision threshold d_{i+1} such that $P(y > d_{i+1} \,|\, P_i) = P_e$. The error probability P_e, assuming equally likely symbols and Gray encoding, is given by

$$P_e \approx {\rm BER} \cdot \log M \frac{M}{2\,(M-1)}. \tag{5}$$

Once we adjust the decision threshold, we can calculate the next level P_{i+1} such that $P(y < d_{i+1} \,|\, P_{i+1}) = P_e$. We repeat these steps until all the levels and decision thresholds are calculated.

We employ an iterative procedure to model a non-ideal modulator extinction ratio. In the first iteration, we assume $P_0 = 0$ to obtain all of the intensity levels. Having obtained the highest intensity level P_{M-1}, we adjust the lowest intensity level P_0 to satisfy $P_0 = r_{\rm ex}\,P_{M-1}$, where $r_{\rm ex}$ is the modulator extinction ratio. We repeat this process until the desired extinction ratio is achieved with reasonable accuracy.

Computing the conditional probabilities naturally depends on the noise statistics. In the particular case that the signal-dependent noise is Gaussian distributed, the conditional probabilities can be easily calculated using Q-functions and the

TABLE I
CHARACTERISTICS OF PUBLISHED APDS

Ref.	Responsivity R 1310 nm (A/ W)	Impact ionization factor k_A	Dark current I_d at $G = 10$ (nA	Low-gain bandwidth / Gain-bandwidth Product (GHz)	Structure and materials
[12]	0.74	0.18	40	24 / 290	Resonant-cavity InGaAs–InAlAs
[13]	0.65	0.2	50*	40 / 115	Waveguide InGaAs–InAlAs
[10]	0.27	0.18–0.27	200	27 / 120	Waveguide InGaAs–InAlAs
[32]	0.17	0.1–0.2	60	28 / 320	Waveguide InGaAs–InAlAs
[14]	0.68	0.15–0.25	1000*	37.5 / 140	Waveguide evanescently coupled photodiode GaInAs–InAlAs
[33]	0.42	0.2	65	27 / 220	p-down inverted InGaAs–InAlAs
[11]	0.55	0.08–0.18	1000	14 / 340	Separate absorption, charge, and multiplication (SACM) Ge–Si

*At 90% of breakdown voltage.

intensity levels are given by [21], [22]:

$$P_k = P_{k-1} + \frac{Q^{-1}\left(P_e\right)}{GR}\left(\sigma_k + \sigma_{k-1}\right), \tag{6}$$

where σ_{k-1}^2 is the noise variance at level $k-1$. Given P_{k-1}, we can determine σ_{k-1} and solve for P_k using (3).

In the more general case, we can use the saddle point approximation [37] to calculate the conditional probabilities for a given conditional MGF Ψ(s):

$$p\left(y > d_{i+1}|P_i\right) \approx \frac{\exp\left(\Phi\left(s_0^+, d_{i+1}\right)\right)}{\sqrt{2\pi\Phi''\left(s_0^+, d_{i+1}\right)}} \tag{7}$$

$$p\left(y < d_i|P_i\right) \approx \frac{\exp\left(\Phi\left(s_0^-, d_i\right)\right)}{\sqrt{2\pi\Phi''\left(s_0^-, d_i\right)}}, \tag{8}$$

where Φ''(s) is the second derivative of the so called phase function Φ(s), which is defined as

$$\Phi\left(s, x\right) = \ln\left(\frac{\Psi\left(s\right)}{|s|}\right) - sx. \tag{9}$$

Here, Ψ(s) is the MGF of y and s_0^+ and s_0^- are the positive and negative saddle points, which are positive and negative roots of $\Phi'\left(s\right) = 0$. As discussed in Section II, for pre-amplified systems, the MGF of y is obtained through a KLSE, which includes the interference of optical and post-detection electrical filter.

Fig. 4 shows, for instance, the conditional probability distribution of $y[k]$ for a pre-amplified system whose signal and ASE components have MGF given in (4). It is evident that the higher intensity levels are subject to higher noise variances. When using equally spaced levels (Fig. 4(a)), the symbol error probability is dominated by the errors at the highest levels. The decision thresholds in this case are at the intersection of the conditional probability density functions in order to minimize the error probability. When the spacing between intensity levels is optimized to approximately equalize the error probability on all intensity levels (Fig. 4(b)), the average power efficiency is improved.

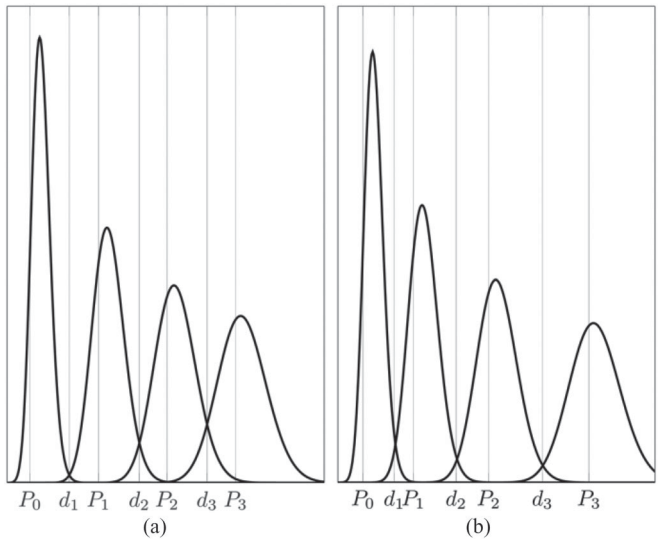

Fig. 4. Conditional probability density function of received samples for a PAM system with (a) equally spaced intensity levels and optimized decision thresholds, and (b) optimized intensity levels and optimized decision thresholds. The conditional distributions are calculated for an SOA with gain G = 20 dB and very low average input power of −30 dBm to clearly show the effects of level optimization.

IV. IMPACT OF COMPONENT LIMITATIONS ON SYSTEM PERFORMANCE

In this section, we study the major component limitations and their impact on the system performance of a single 100 Gbit/s channel. More specifically, we model and analyze the effects of SOA gain saturation, modulator bandwidth, and APD excess noise and gain-bandwidth product. In this section, we consider a single-wavelength link operating near the dispersion zero at 1310 nm. We analyze WDM systems and the combined effect of chirp and CD in Section V.

Throughout this paper, we quantify the system performance relative to an ideal ISI-free 107-Gbit/s 4-PAM system with a thermal noise-limited PIN receiver. The receiver sensitivity of the reference system can be computed as a function of the target BER [1]:

$$\bar{P}_{\mathrm{req,ref}} = \sqrt{\frac{R_b S_{\mathrm{th}}(M-1)^2}{2R^2\log_2 M}}\, Q^{-1}\left(\frac{M\log_2 M \mathrm{BER}_{\mathrm{target}}}{2\left(M-1\right)}\right). \tag{10}$$

where R_b is the bit rate and R is the photodiode responsivity. For our analysis and simulation in this paper, we assume $R_b = 107\,\mathrm{Gbit/s}$, $R = 1\,\mathrm{A/W}$, and a TIA with $\bar{I}_{n,\mathrm{in}} = 30\,\mathrm{pA}/\sqrt{\mathrm{Hz}}$. Hence, for $\mathrm{BER}_{\mathrm{target}} = 1.8\times10^{-4}$, the reference receiver sensitivity is $\bar{P}_{\mathrm{req,ref}} \approx -13$ dBm.

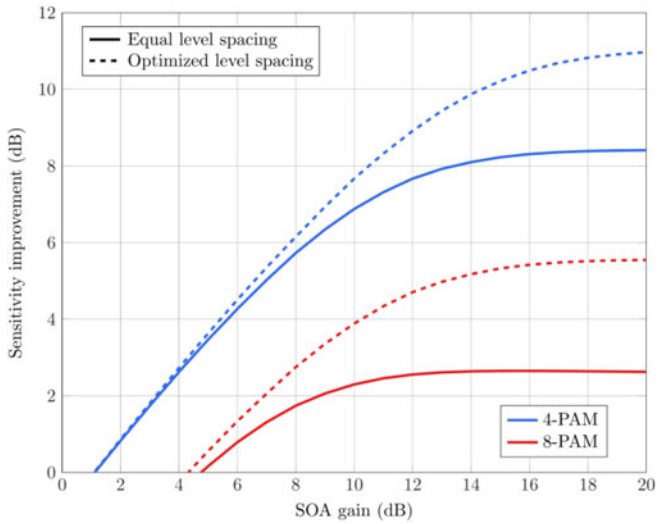

Fig. 5. Receiver sensitivity improvement versus SOA gain for 4- and 8-PAM systems with equal and optimized level spacing. The reference system is an ideal ISI-free, thermal noise-limited receiver for 4-PAM at $\mathrm{BER} = 1.8 \times 10^{-4}$. We consider an SOA noise figure of 6 dB. Increasing the noise figure by 1 dB reduces the sensitivity improvement by about 1 dB.

A. SOA-Based Receiver

1) SOA Gain: Using the model described in Section II-B, we can evaluate the effects of the gain of a linear SOA on the performance of a system with negligible ISI (using an ideal wide-band modulator). Fig. 5 shows the receiver sensitivity improvement as we vary the gain of an SOA with noise figure $F_n = 6$ dB. As can be seen in Fig. 5, a high-gain SOA can improve the receiver sensitivity by more than 8 dB. We find that using optimized intensity levels further improves receiver sensitivity by ~2 dB compared to equally spaced levels. In Fig. 5, we only show the sensitivity improvements for an amplifier with $F_n = 6$ dB; however, we note that a 1-dB reduction of F_n leads to ~1 dB improvement in the receiver sensitivity.

A key observation is that for typical values of SOA fiber-to-fiber gain (20-30 dB), receiver sensitivity is insensitive to the gain as long as the system is remains in the ASE-dominated regime. As discussed in Section V, this is particularly important for WDM links, since the SOA gain is dependent on the temperature, signal wavelength and power.

In Fig. 5 we show the results for a linear amplifier, however, an SOA when operating in the saturation regime, can introduce pattern-dependent self-gain modulation in single-wavelength links and inter-channel crosstalk in WDM links, potentially compromising receiver sensitivity improvements [38]–[40]. The impact of gain saturation can be decomposed into a steady-state gain reduction related to the average input power and gain fluctuations due to random variation of the total input power [39]. The impact of gain fluctuations on system performance is strongly dependent on the SOA carrier lifetime. Self-gain modulation is reduced if the symbol rate is much larger than the reciprocal of the carrier lifetime. However, crosstalk and ISI due to cross-gain modulation is known to be problematic in WDM systems [39].

SOA gain dynamics can be well-modeled by rate equations governing carrier density N and optical power P. The rate equations can be used to obtain the following differential equation for optical gain coefficient g [41]

$$\frac{\partial g}{\partial t} = \frac{g_0 - g}{\tau_c} - \frac{g}{\tau_c}\frac{P}{P_{\mathrm{sat}}}, \tag{11}$$

where τ_c the is carrier lifetime, $\mathrm{P_{sat}}$ is the saturation power, and $\mathrm{g_0}$ is the unsaturated optical gain coefficient. Following [41], we integrate (11) over the amplifier length to obtain

$$\left(1 + \tau_c \frac{d}{dt}\right) h(t) = g_0 L - \frac{P_{\mathrm{in}}(t)}{P_{\mathrm{sat}}} \left(\exp(h) - 1\right), \tag{12}$$

where L is the amplifier length and $h(t)$ is defined as

$$h(\tau) = \int_0^L g(z, \tau)\, dz. \tag{13}$$

In steady state, (13) reduces to a well-known expression for amplifier gain $G = \exp(h)$ as a function of input power:

$$P = \frac{P_{\mathrm{sat}}}{G - 1} \ln \frac{G_0}{G}, \tag{14}$$

where $G_0 = \exp(g_0 L)$ is the unsaturated amplifier gain.

Similar to small-signal analysis in [42], [43], we assume the input power $P_{\mathrm{in}}(t)$ and $h(t)$ fluctuate around their steady-state values and can be represented by

$$\begin{aligned} P_{\mathrm{in}}(t) &= \overline{P}_{\mathrm{in}} + \delta P_{\mathrm{in}}(t) \\ h(t) &= \overline{h} + \delta h(t). \end{aligned} \tag{15}$$

Using (15) and assuming $\exp(h) >> 1$, we can simplify (12) and derive a linear differential equation

$$\left(1 + \frac{\tau_c}{1+\eta}\frac{d}{dt}\right) \delta h(t) = -\frac{\eta}{1+\eta}\frac{\delta P_{\mathrm{in}}(t)}{\overline{P}_{\mathrm{in}}}, \tag{16}$$

where η is a gain compression factor [42]

$$\eta \approx h_0 - \overline{h} = \frac{\overline{P}_{\mathrm{in}}}{P_{\mathrm{sat}}}\left(e^{\overline{h}} - 1\right) \approx \frac{\overline{P}_{\mathrm{in}}}{P_{\mathrm{sat}}} e^{\overline{h}}, \tag{17}$$

which describes the steady-state saturated gain relative to the unsaturated gain of the amplifier. Equation (16) is a first-order differential equation, with a solution given by

$$\delta h(t) = -\frac{\eta}{1+\eta}\frac{\langle \delta P_{\mathrm{in}}(t) \rangle}{\overline{P}_{\mathrm{in}}}, \tag{18}$$

where $\langle P_{\mathrm{in}}(t) \rangle$ denotes an exponentially weighted moving average of the input power with a window

$$w(t) = (1+\eta) \exp\left(-(1+\eta)\frac{t}{\tau_c}\right) u(t), \tag{19}$$

and can obtained by the convolution $\langle P_{\mathrm{in}}(t) \rangle = P_{\mathrm{in}}(t) * w(t)$. Equation (19) shows that the small-signal response of the gain to input power variations is similar to a low-pass filter with time constant $\tau_c/(1+\eta)$. Hence, for SOAs with carrier lifetime much larger than the symbol duration, the amplifier gain is almost constant, and is determined by the average power.

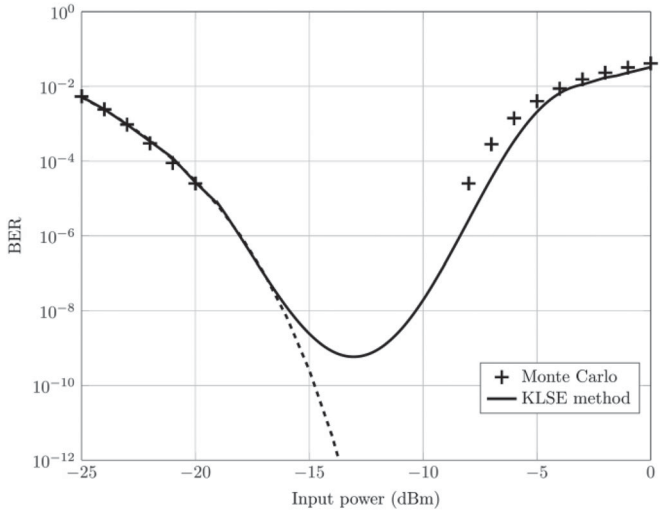

Fig. 6. BER versus input power in presence of transient gain saturation in a single-wavelength 100 Gbit/s 4-PAM link. The dashed line corresponds to the BER in the absence of gain saturation. Results assume a saturation power $\mathrm{P_{sat}} = +15\,\mathrm{dBm}$ and a carrier lifeitme $\tau_c = 200\,\mathrm{ps}$.

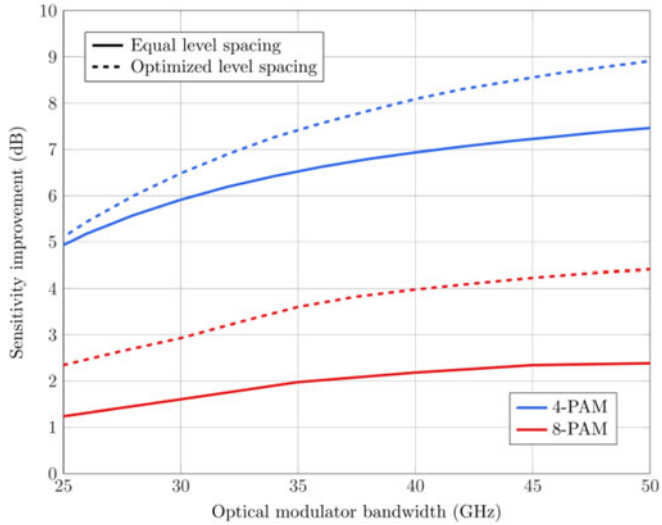

Fig. 7. Receiver sensitivity improvement versus modulator 3-dB bandwidth for 4- and 8-PAM systems with equal and optimized level spacings. We consider an SOA with unsaturated gain $\mathrm{G_0} = 20\,\mathrm{dB}$ and noise figure $\mathrm{F_n} = 6\,\mathrm{dB}$ and a modulator with extinction ratio of $\mathrm{r_{ex}} = -10\,\mathrm{dB}$.

Using the small-signal response of the gain, we can derive a simple expression for G:

$$\langle P_{\mathrm{in}}(t)\rangle = \frac{P_{\mathrm{sat}}}{G-1}\ln\frac{G_0}{G}. \tag{20}$$

Note that for links with multiple WDM channels, $\langle P_{\mathrm{in}}(t)\rangle$ is the sum of the average powers of individual channels. Assuming symbols in different channels are uncorrelated, the gain fluctuations are smaller than for a single channel with the same average power. Therefore, gain fluctuations become increasingly negligible as the number of WDM channels increases. In high-speed WDM links, typically, crosstalk due to gain variation is negligible and steady-state gain reduction is the dominant effect, whereas ISI due to self-gain modulation becomes important in signal-wavelength links [39].

Using the model described above, we evaluate the impact of self-gain modulation in single-wavelength 100 Gbit/s links, comparing numerical analysis to Monte Carlo simulation. We assume a typical SOA with carrier life time of 200 ps [43], corresponding to ∼10 symbol intervals assuming 4-PAM.

For the Monte Carlo simulation, we use (20) to calculate the instantaneous gain of the amplifier and then calculate the output power by $P_{\mathrm{out}}(t) = G(t)\,P_{\mathrm{in}}(t)$. To capture the effect of the long memory of the SOA, we simulate detection of a pseudorandom bit sequence of length $2^{20} - 1$ generated by a linear feedback shift register with 20 taps.

For the analysis, we numerically solve the differential equation (16) to calculate the nonlinear response of the SOA to an arbitrary modulated input signal and expand the output signal using KLSE method to obtain the MGF of the detected samples. To calculate the BER, we use M-ary De Bruijn sequence of order $n = 5$.

Fig. 6 shows the BER of a single-wavelength 100 Gbit/s link as function of input power. We show only results for 4-PAM, as De Bruijn sequences with order sufficient to span the long SOA memory are prohibitively long for 8-PAM. As illustrated in Fig. 6, gain saturation significantly degrades dynamic range of the optical power. If the dynamic range (∼15 dB in Fig. 6) is insufficient, the link can employ a variable optical attenuator to limit the received power. Alternatively, the interference caused by transient gain saturation can be mitigated using a gain-clamped SOA [20], [44] or an SOA with increased carrier life time [43].

2) Modulator Bandwidth: In present 100 Gbit/s-per-wavelength links, modulator bandwidths are significantly lower than the symbol rate, causing ISI that necessitates digital compensation of the modulator frequency response to mitigate performance degradation.

In SOA-based receivers with wideband optical filtering, the modulator bandwidth is the dominant source of bandwidth limitation. Since the bandwidth of the optical filter is typically significantly higher than the optical signal bandwidth, we neglect the effect of this filter on the received pulse shape in computing the matched filter.

In order to apply the KLSE method, we use the overall response of the matched filter and the equivalent continuous-time impulse response of the discrete-time LE. Fig. 7 shows the impact of modulator bandwidth in pre-amplified systems. Comparing to ISI-free system (Fig. 5), there is additional penalty of about 1.5 dB for a 4-PAM system using a modulator with 30-GHz bandwidth, which is caused mainly by noise enhancement. We observe that the improvement achieved by optimizing the intensity levels and decision thresholds is smaller for lower modulator bandwidths. This is mainly because in the presence of ISI, the received signal-dependent noise in each sample depends on a weighted average over several symbols and hence, the optimized levels are closer to equally spaced levels.

As mentioned before, in practice, a fixed anti-aliasing filter followed by an ADC with sampling rate slightly higher than the symbol rate is used. Digital equalization can be done either in

the time or the frequency domain. The performance of a well-designed LE with fixed anti-alias filtering and oversampling can approach the performance of the ideal symbol-rate LE analyzed here. In simulations, we observe worst case penalty of 1 dB and 0.4 dB for oversampling ratios of $5/4$ and 2 respectively.

B. APD-Based Receiver

In an APD-based receiver signal power scales with G^2, while shot noise variance scales with G^3, as can be seen from (3). This implies that increasing the APD gain after shot noise becomes dominant hurts receiver sensitivity. Therefore, there is an optimal APD gain that minimizes receiver sensitivity, and this gain lies below the range at which shot noise becomes completely dominant.

Moreover, in the avalanche buildup time limited regime, the APD gain and bandwidth are coupled and relatd by the GBP. Hence, to determine the optimal APD gain we must account for APD bandwidth limitations.

The APD filters both signal and shot noise. Consequently, the total noise (shot plus thermal noise) is not white. From Fig. 2(b), the shot noise component of the decision variable $y[n]$ is given by

$$y_{n,\mathrm{sh}}[k] = h(t) * n_{\mathrm{sh}}(t)\,|_{t=kT_s}\ , \tag{21}$$

where $h(t) = h_{\mathrm{APD}}(t) * h_e(t)$, and the electrical filter $h_e(t)$ comprises of a noise-whitening filter, a matched filter matched to the received pulse shape, and the continuous-time equivalent of the discrete-time LE. $n_{\mathrm{sh}}(t)$ is the shot noise, whose PSD is given by (3). It thus follows that

$$\begin{aligned}\mathrm{Var}\left(y_{n,\mathrm{sh}}[k]\right) &= \left[2qG^2F_A(G)\left(RP_{\mathrm{rx}}(t)+I_d\right)\right] \\ &\quad * |h(t)|^2\,|_{t=kT_s}\end{aligned} \tag{22}$$

Note that the received intensity waveform $P_{\mathrm{rx}}(t)$ already includes ISI caused by the modulator. Thus, $P_{\mathrm{rx}}(t) = x(t) * h_{\mathrm{mod}}(t)$, where $x(t)$ is the ISI-free modulator drive signal, and $h_{\mathrm{mod}}(t)$ is the modulator impulse response.

If shot noise were signal-independent, the convolution in (22) would reduce to simply scaling the noise variance by the energy of $h(t)$, leading to the well-known noise enhancement penalty. Here, however, the convolution in (22) makes the noise variance dependent on the sequence of symbols within the memory length of $|h(t)|^2$. Fortunately, the memory length of $|h(t)|^2$ is fewer than five symbols, even when the APD bandwidth is as low as 20 GHz. The impact of $|h(t)|^2$ on the shot noise variance is particularly noticeable on the lowest intensity levels. As an example, the variance of the shot noise component $y_{n,\mathrm{sh}}[k]$ is nonzero even when the symbol $P_0 = 0$ is transmitted (modulation with an ideal extinction ratio), due to shot noise from neighboring symbols.

In performing level spacing optimization, we adopt a conservative approach and calculate (22) considering the worst-case scenario, where all the symbols in the memory of $|h(t)|^2$ are the highest level P_{M-1}.

The effect of thermal noise can be computed in terms of its equivalent one-sided noise bandwidth, since thermal noise is not signal-dependent. Hence, $\sigma^2_{\mathrm{th}} = S_{\mathrm{th}}\Delta f_{\mathrm{th}}$, where

$$\Delta f_{\mathrm{th}} = \int_0^\infty |H_e(f)|^2 df, \tag{23}$$

and $H_e(f)$ is the electric filter frequency response. We have assumed $H_e(0) = 1$.

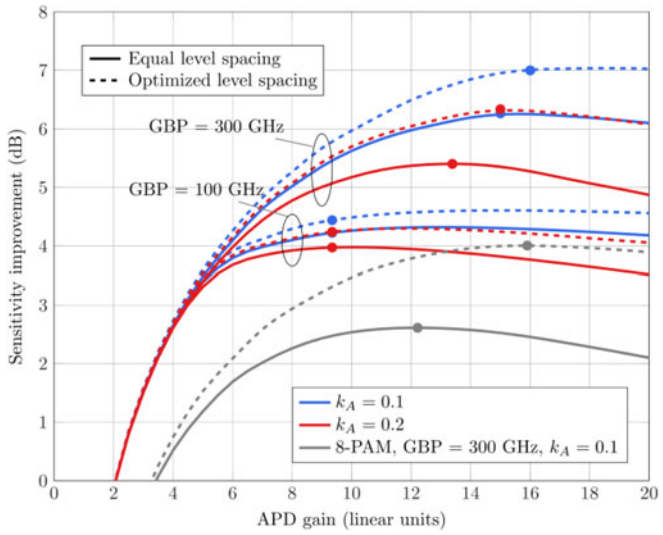

Fig. 8. Receiver sensitivity improvement versus APD gain for 4-PAM and $k_A = 0.1$ (Si) and $k_A = 0.2$ (InAlAs) and two values of GBP: 100 GHz and 300 GHz. The 8-PAM best-case scenario is shown for reference. Results assume $\mathrm{R_b} = 107\,\mathrm{Gbit/s}$, $\mathrm{RIN} = -150\,\mathrm{dB/Hz}$, $\mathrm{I_d} = 100\,\mathrm{nA}$ at $\mathrm{G} = 10$, $r_{\mathrm{ex}} = -10$ dB, $\bar{I}_{n,\mathrm{in}} = 30\mathrm{pA}/\sqrt{\mathrm{Hz}}$, APD low-gain bandwidth of 20 GHz, $f_{\mathrm{mod},3dB} = 30\mathrm{GHz}$. Circles indicate optimal gains.

Fig. 8 shows the sensitivity improvements for 4-PAM as a function of the APD gain for two different GBP scenarios: 100 GHz and 300 GHz. Curves for 8-PAM are included for the best scenario only. We assume the APD has the same responsivity as the reference system, i.e., $R = 1\mathrm{A/W}$, but the results in Fig. 8 can be easily converted to $R \neq 1$ A/W by appropriately shifting the curves vertically. For instance, for $R = 0.5$ A/ W, the sensitivity improvements would be 3 dB lower than those presented in Fig. 8.

For GBP = 100 GHz, avalanche buildup time limits the bandwidth when $G \geq 5$. In this regime, increasing the gain further reduces the APD bandwidth, but this does not translate into an increased noise enhancement penalty, since the APD filters both signal and shot noise. As a result, the sensitivity improvement remains almost constant.

For GBP = 300 GHz, the avalanche buildup time-limited regime is reached at higher gains, when $G \geq 15$, and hence higher sensitivity improvements can be achieved. For $k_A = 0.1$ we observe sensitivity improvements up to 6.3 dB for equal level spacing, and up to 7 dB for optimized levels. Note, however, that there is very little penalty by operating the APD at gains substantially smaller than the optimal gain.

Although 8-PAM is more spectrally efficient than 4-PAM, its poorer noise tolerance leads to significantly smaller sensitivity improvements in both SOA- (Fig. 7) and APD-based systems

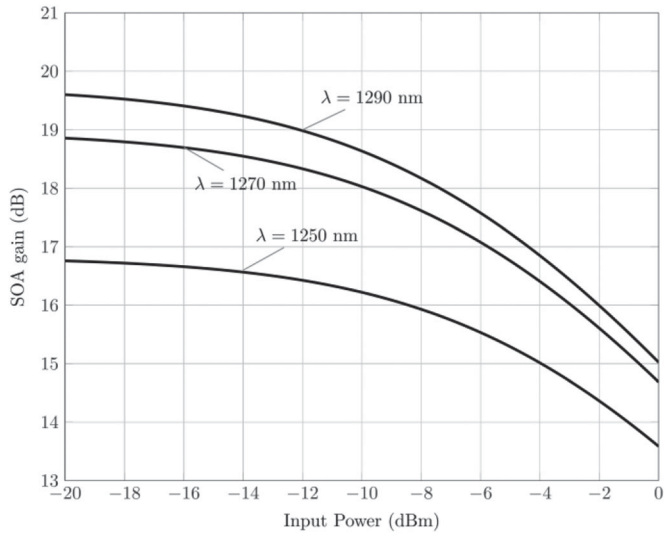

Fig. 9. Gain saturation characteristics of SOA with unsaturated peak gain of $G_0 = 20$ dB at 1290 nm and saturation power $P_{sat} = +15\,dBm$.

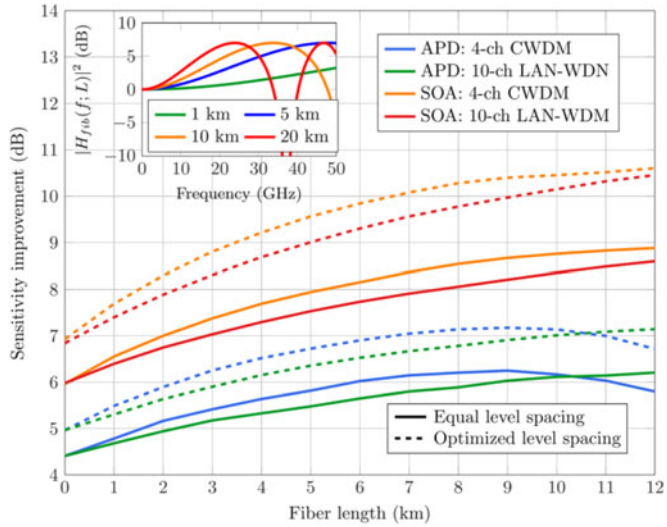

Fig. 10. Receiver sensitivity improvement versus fiber length for 4-PAM. SOA curves assume a SOA with unsaturated peak gain of $G_0 = 20\,dB$ and noise figure $F_n = 6\,dB$ and an optical modulator bandwidth $f_{3dB} = 30\,GHz$. The APD parameters assumed are listed in Table I and taken from [12]. All of the other parameters assumed are listed in Table II.

(Fig. 8). Hence, as in systems using PIN-based receivers [1], 4-PAM outperforms 8-PAM.

V. WDM System Performance

In this section, we evaluate the performance of 100 Gbit/s-per-wavelength WDM links. The performance of individual channels could be different due to wavelength-dependent characteristics of the system such as CD. The WDM analysis is particularly important for receivers with SOAs to evaluate the effects of wavelength-dependent gain and nonlinear crosstalk caused by cross-gain modulation

The amount of dispersion that each channel experiences depends on the channel spacing as well as the number of channels. The typical channel spacing for short-reach applications is 20 nm for CWDM links and 4.5 nm for LAN-WDM. Although CWDM is often preferred, as it generally does not require temperature-controlled lasers, LAN-WDW can accommodate more channels close to the zero-dispersion wavelength, which is necessary for 1 Tbit/s and possibly $1.6\,Tbit/s$ systems.

The number of channels in the short-reach WDM links considered here, is typically constrained by transmit power limit (and possibly SOA bandwidth), as opposed to chromatic dispersion. Here, we consider two systems: 10-channel LAN-WDM with 4.5-nm channel spacing and 4-channel CWDM with 20-nm channel spacing. The average optical power launched in to the fiber is limited to 9.4 dBm due to eye-safety restrictions. Therefore, for 4- and 10-channel WDM links, the average transmitted optical power per channel cannot exceed 3.4 dBm and -0.6 dBm, respectively. Thus, even if the 4- and 10-channel systems have relatively similar receiver sensitivities, the 10-channel LAN-DWM has $\sim$4 dB lower link margin than the 4-channel CWDM.

The performance degradation caused by dispersion depends on the characteristics of laser frequency chirp. Transient chirp is dominant in both high-speed DMLs [45] and EAMs [46]. In direct detection systems, the combination of chirp and CD introduces nonlinear distortion. However, for short propagation distances, their combined impact can be modeled as a linear filter with small-signal frequency response of [47]

$$H_{\text{fib}}(f;L) = \cos\theta - \alpha\sin\theta, \tag{24}$$

We use (24) in the design of the LE to partially compensate for the impact of CD. Note that the linear approximation in (24) is only valid when the signal and the parameter θ are suitably small. Hence, the LE is only effective for link lengths of a few kilometers. For longer link lengths, however, modulator chirp and CD cause severe nonlinear distortion that cannot be compensated by the LE.

Note that for small propagation distances, based on (24), systems with $\alpha D(\lambda) > 0$ are subject to severe power fading. However, for systems $\alpha D(\lambda) < 0$, the second term in (24) is negative, which provide some gain (see inset in Fig. 10). This gain can potentially compensate the frequency response of the modulator and APD. Therefore, we assume all of the WDM channels are placed at wavelengths shorter than the zero-dispersion wavelength (1310 nm for standard SMF), such that $\alpha D(\lambda) < 0$ is satisfied for modulator with positive chirp.

SOA gain is another wavelength-dependent parameter that can limit the performance of WDM links. As mentioned before, a single SOA can amplify multiple WDM channels, but the amplifier gain is different for each channel, as g depends on wavelength. In order to model this dependence, we use a cubic formula as suggested in [48]:

$$g(\lambda, N) = g(N) - \gamma_1(\lambda - \lambda_N)^2 + \gamma_2(\lambda - \lambda_N)^3, \tag{25}$$

where λ_N is the wavelength of the peak gain, and γ_1 and γ_2 are constants determined to fit the experimentally measured SOA in [19], which has 3-dB gain bandwidth of $\sim$80 nm. We further assume an SOA with peak gain of $\sim$20 dB at a wavelength at the center of the WDM spectrum, which can be

TABLE II
SIMULATION PARAMETERS

System	R_b	107 Gb/ s
	PAM order	4
	$\mathrm{BER}_{\mathrm{target}}$	1.8×10^{-4}
Mod	$f_{3\mathrm{dB}}$	30 GHz
	r_{ext}	–10 dB
	RIN	– 150 dB/ Hz
	α	2
SMF	S_0	0.092 ps/(nm^2 km)
	λ_0	1310 nm
Optical filter	type	5$^{\mathrm{th}}$ order Bessel
	Bandwidth (BW)	400 GHz
SOA	G_0	20 dB
	P_{sat}	+15 dBm
	τ_c	200 ps
	λ_N	1290 nm
	γ_1	7.7 nm^{-2}
	γ_2	0.02 nm^{-3}
APD	R	0.74 A/ W
	Low-gain BW	20 GHz
	Dark current	100 nA @ G = 10
TIA	I_n	$30\,\mathrm{pA}/\sqrt{\mathrm{Hz}}$

achieved by choice of the active layer composition. Fig. 9 shows gain saturation curves for three different wavelengths. Table II summarizes other parameters used in the analysis and simulations.

Fig. 10 shows the receiver sensitivity improvement versus the optical fiber length for both WDM links and both type of receivers. For each system, we only show the performance at the wavelength subject to the highest dispersion (1250 nm for CWDM and 1270 nm for LAN-WDM, assuming one of the channels is at the zero-dispersion wavelength). The results can be simply scaled to evaluate the performance of a channel at a different wavelength. For both WDM links, as shown in Fig. 10, SOA-based receiver outperforms their APD-based counterparts, mainly due to the limited responsivity of the APDs.

Another observation in Fig. 10 is that for short link lengths, modulator chirp and CD actually improve the sensitivity of both types of receivers. This is due to the gain in the dispersion-induced frequency response of the channel, which partially compensates the LE noise enhancement penalty. For a 5-km link, the receiver sensitivity is improved by about 8 dB and 6 dB for SOA- and APD-based CWDM receivers respectively with equally spaced levels. The improvement is less significant for LAN-WDM receivers as these systems experience less dispersion. For longer link lengths, however, modulator chirp and CD cause severe nonlinear distortion that cannot be compensated by a LE.

VI. PRACTICAL CONSIDERATIONS

Temperature sensitivity and power consumption are important practical considerations in data center applications.

For SOAs, increasing temperature generally reduces the gain and saturation power and shifts the gain peak toward longer wavelengths. The gain of InGaAsP SOAs can vary as much as -0.3 dB/ °C with temperature [6], [7], whereas GaInNAs SOAs have superior temperature stability with gain variations of about $-0.04\,\mathrm{dB}/^{\circ}\mathrm{C}$ [49], [50], which may enable CWDM links with uncooled SOAs to operate over wider temperature ranges.

In single-wavelength links, the combined red shift and decrease of the peak gain can be exploited to achieve gain variations of just a few dB over the temperature range 20–70 °C [49], [51], [52], which results in a negligible performance penalty. For CWDM links the temperature sensitivity of SOAs is paramount, as the gain for the shortest-wavelength channel may drop abruptly with increasing temperature, particularly in InGaAsP SOAs. In [49], [50], the gain decrease exceeded 10 dB at 50 °C, causing a power penalty of $\sim$1 dB. Operation at temperatures above $\sim$50 °C would likely require SOA cooling.

Temperature sensitivity in APDs is more manageable than in SOAs. Breakdown voltage variations over temperature can be compensated through active APD bias control. The breakdown voltage thermal coefficient is $70\%/^{\circ}\mathrm{C}$ for InAlAs-based APDs, but only $0.05\%/^{\circ}\mathrm{C}$ for Si-based APDs [11]. APD-based systems can operate over wide temperature ranges with small sensitivity variations, e.g., a commercial 10 Gbit/s receiver can operate over a $0^{\circ}\mathrm{C}-75^{\circ}\mathrm{C}$ range with only 1-dB penalty at $\mathrm{BER} = 10^{-12}$ [9].

Compared to SOAs, APDs are low-power devices with power consumption of the order of 1 mW for typical values of input optical power $P_{\mathrm{rx}} \sim -15$ dBm and bias voltage $V_{\mathrm{bias}} \sim -25\mathrm{V}$. Commercial SOAs with TECs have power consumption of $\sim$1 W [51], [53] while uncooled SOAs have power consumption of few hundreds of mW [51].

VII. CONCLUSION

We have evaluated the performance of 4-PAM and 8-PAM 100 Gbit/s per-wavelength links using SOAs or APDs to improve receiver sensitivity and using LE to compensate for ISI caused by the modulator and APD. We have shown that, as in PIN-based receivers, 4-PAM outperforms 8-PAM due to its higher noise tolerance.

We modeled key link impairments including modulator bandwidth limitations and chirp, fiber CD, transient SOA gain saturation, excess shot noise and ISI caused by the APD. We found that in a 4-PAM link using LE, an SOA with noise figure $F_n = 6$ dB can improve receiver sensitivity by up to 6 dB with respect to an ideal ISI-free thermal-noise limited PIN receiver. Transient gain saturation has a negligible impact on receiver sensitivity, but limits the receiver dynamic range to about 15 dB for the worst case of single-wavelength amplification.

APD-based receivers may provide sensitivity improvements up to 4 dB for GBP = 100 GHz, and up to 6.2 dB for GBP = 300 GHz, assuming a low-gain bandwidth of 20 GHz, $k_A = 0.1$ (Si). APDs fabricated in InAlAs ($k_A = 0.2$) with otherwise the same characteristics may provide sensitivity improvements up to 5.3 dB. These sensitivity improvement values are with respect to an ideal thermal-noise limited PIN receiver with same responsivity. Unfortunately, however, current APDs still have responsivities below $1\,\mathrm{A}/\mathrm{W}$, which reduce the achievable sensitivity, e.g., by 3 dB for Ge–Si APDs having $R = 0.5$ A/ W

and by 1.3 dB for InGaAs–InAlAs having $R = 0.74\,\mathrm{A/W}$ (Table I). Hence, current resonant-cavity or waveguide InGaAs–InAlAs APDs offer better tradeoff between k_A, responsivity, and GBP than Ge–Si APDs. As an example, the resonant-cavity InGaAs–InAlAs from [12] has a sensitivity improvement of 4.5 dB over the reference system.

Optimization of the PAM level spacing and receiver decision thresholds can provide about 1 to 2 dB additional sensitivity improvement for either SOA and APD-based receivers. Moreover, by appropriately selecting wavelengths such that $\alpha D(\lambda) < 0$, the receiver sensitivity is improved after a few km of fiber, due to the combined effect of CD and modulator chirp.

SOA-based receivers offer higher sensitivity improvement than APD-based receivers, owing particularly to the poor responsivity of current APDs. Moreover, SOAs can amplify multiple WDM channels, helping amortize their higher cost and power dissipation. Important practical considerations such as cost, temperature sensitivity, and power consumption may nonetheless favor APDs in practical systems.

ACKNOWLEDGMENT

The authors would like to thank the helpful discussions with A. Shastri and J. Filip.

REFERENCES

[1] M. Sharif, J. K. Perin, and J. M. Kahn, "Modulation schemes for single-laser 100 Gb/s links: Single-carrier," *J. Lightw. Technol.*, vol. 33, no. 20, pp. 4268–4277, Oct. 2015.

[2] J. K. Perin, M. Sharif, and J. M. Kahn, "Modulation schemes for single-wavelength 100 Gbit/s links: Multicarrier," *J. Lightw. Technol.*, vol. 33, no. 24, pp. 5122–5132, Dec. 2015.

[3] J. D'Ambrosia, "IEEE P802.3bs baseline summary," [Online]. Available: http://www.ieee802.org/3/bs/index.html, 2015.

[4] D. R. Zimmerman and L. H. Spiekman, "Amplifiers for the masses: EDFA, EDWA, and SOA amplets for metro and access applications," *J. Lightw. Technol.*, vol. 22, no. 1, pp. 63–70, Jan. 2004.

[5] P. P. Iannone, Kenneth, C. Reichmann, and L. Spiekman, "In-service upgrade of an amplified 130-km metro CWDM transmission system using a single LOA with 140-nm bandwidth," in *Proc. Opt. Fiber Commun. Conf.*, vol. 2, Apr. 2003, pp. 548–550.

[6] C. Holtmann, P. A. Besse, T. Brenner, and H. Melchior, "Polarization independent bulk active region semiconductor optical amplifiers for 1.3 micron wavelengths," *IEEE Photon. Technol. Lett.*, vol. 8, no. 3, pp. 343–345, Mar. 1996.

[7] L. F. Tiemeijer, P. J. A. Thijs, T. V. Dongen, J. J. M. Binsma, E. J. Jansen, and A. J. M. Verboven, "27-dB Gain unidirectional 1300-nm polarization-insensitive multiple quantum well laser amplifier module," *IEEE Photon. Technol. Lett.*, vol. 6, no. 12, pp. 1430–1432, Dec. 1994.

[8] M. J. Connelly, *Semiconductor Optical Amplifiers*. Norwell, MA, USA: Kluwer, 2002.

[9] H. Nie, "High performance, low-cost PIN, APD receivers in fiber optical networks and FTTx applications," in *Proc. 14th Annu. Wireless Opt. Commun. Conf.*, 2005, p. 94.

[10] G. S. Kinsey, C. C. Hansing, A. L. Holmes, B. G. Streetman, J. C. Campbell, and A. G. Dentai, "Waveguide InGaAs–InAlAs avalanche photodiode," *IEEE Photon. Technol. Lett.*, vol. 12, no. 4, pp. 416–418, Apr. 2000.

[11] Y. Kang *et al.*, "Monolithic germanium/silicon avalanche photodiodes with 340 GHz gain–bandwidth product," *Nature Photon.*, vol. 3, pp. 59–63, 2009.

[12] C. Lenox, H. Nie, P. Yuan, G. Kinsey, A. L. Homles, B. G. Streetman, and J. C. Campbell, "Resonant-cavity InGaAs-InAlAs avalanche photodiodes with gain-bandwidth product of 290 GHz," *IEEE Photon. Technol. Lett.*, vol. 11, no. 9, pp. 1162–1164, Sep. 1999.

[13] S. Xie, S. Zhang, and C. H. Tan, "InGaAs/InAlAs avalanche photodiode with low dark current for high-speed operation," *IEEE Photon. Technol. Lett.*, vol. 27, no. 16, pp. 1745–1748, Aug. 2015.

[14] V. Makita, T. Nakata, K. Shiba, and T. Takeuchi, "40-Gbps waveguide avalanche photodiodes," *NEC J. Adv. Technol.*, vol. 2, no. 3, pp. 234–240, 2005.

[15] T. Liow, N. Duan, A. E. Lim, X. Tu, M. Yu, and G. Lo, "Waveguide Ge/Si avalanche photodetector with a unique low-height-profile device structure," in *Proc. Opt. Fiber Commun. Conf. Exhib.*, 2014, Paper M2G.6.

[16] M. M. Hayat *et al.*, "Gain-bandwidth characteristics of thin avalanche photodiodes," *IEEE Trans. Electron Dev.*, vol. 49, no. 5, pp. 770–781, May 2002.

[17] M. M. Hayat and D. A. Ramirez, "Multiplication theory for dynamically biased avalanche photodiodes: New limits for gain bandwidth product," *Opt. Express*, vol. 20, no. 7, 2012, Art. no. 8024.

[18] G. El-howayek and M. M. Hayat, "Error probabilities for optical receivers that employ dynamically biased avalanche photodiodes," *IEEE Trans. Commun.*, vol. 63, no. 9, pp. 3325–3335, Sep. 2015.

[19] P. Mazurek, P. Czyzak, H. de Waardt, and J. P. Turkiewicz, "Up to 112 Gbit/s single wavelength channel transmission in the 1310 nm wavelength domain," *Microw. Opt. Technol. Lett.*, vol. 56, no. 2, pp. 263–265, 2014.

[20] T. K. Chan and W. I. Way, "112 Gb/s PAM4 transmission over 40 km SSMF using 1.3 μm gain-clamped semiconductor optical amplifier," in *Proc. Opt. Fiber Commun. Conf. Exhib.*, 2015, pp. 1–3.

[21] T. V. Muoi and J. L. Hullett, "Receiver design for multilevel digital optical fiber systems," *IEEE Trans. Commun.*, vol. 23, no. 9, pp. 987–994, Sep. 1975.

[22] H. Keangpo and J. Kahn, "Multilevel optical signals optmized for systems having signal-dependent noises, finite transmitter extinction ratio and intersymbol interference," U.S. Patent US6690894 B2 vol. 2, no. 12, Feb, 10, 2004.

[23] T. Yamamoto, "High-speed directly modulated lasers," in *Proc. Opt. Fiber Commun. Conf. Expo./Nat. Fiber Opt. Eng. Conf.*, 2012, pp. 1–39.

[24] N. Kikuchi, R. Hirai, and T. Fukui, "Practical implementation of 100-Gbit/s/Lambda optical short-reach transceiver with nyquist PAM4 signaling using electroabsorptive modulated laser (EML)," in *Proc. Opt. Fiber Commun. Conf. Exhib.*, 2015, pp. 1–3.

[25] M. N. Ahmed, *Transimpedance Amplifier (TIA) Design for 400 Gb/s Optical Fiber Communications*. Blacksburg, VA, USA: Virginia Polytechnic Institute and State University, 2013.

[26] S. Bates, M. Gustlin, and J. Slavick, "FEC options," IEEE P802.3bj, Newport Beach, CA, USA, pp. 1–11, 2011.

[27] Z. Wang and A. Ghiasi, "FEC tradeoffs and analyses for 100G optical networking," IEEE 802.3bm, Geneva, pp. 1–7, 2012.

[28] A. E. Kelly *et al.*, "High-performance semiconductor optical amplifier modules at 1300 nm," *IEEE Photon. Technol. Lett.*, vol. 18, no. 24, pp. 2674–2676, Dec. 2006.

[29] E. Forestieri, "Evaluating the error probability in lightwave systems with chromatic dispersion, arbitrary pulse shape and pre- and postdetection filtering," *J. Lightw. Technol.*, vol. 18, no. 11, pp. 1493–1503, Nov. 2000.

[30] E. Forestieri and M. Secondini, "On the error probability evaluation in lightwave systems with optical amplification," *J. Lightw. Technol.*, vol. 27, no. 6, pp. 706–717, Mar. 2009.

[31] C. W. Helstrom, "Approximate evaluation of detection probabilities in radar and optical communications," *IEEE Trans. Aerosp. Electron. Syst.*, vol. AES-14, no. 4, pp. 630–640, Jul. 1978.

[32] G. S. Kinsey, J. C. Campbell, and A. G. Dentai, "Waveguide avalanche photodiode operating at 1.55 um with a gain-bandwidth product of 320 GHz," *IEEE Photon. Technol. Lett.*, vol. 13, no. 8, pp. 842–844, Aug. 2001.

[33] M. Nada, Y. Muramoto, H. Yokoyama, N. Shigekawa, T. Ishibashi, and S. Kodama, "Inverted InAlAs/InGaAs avalanche photodiode with low-high-low electric field profile," *Jpn. J. Appl. Phys.*, vol. 51, no. 2 Part 2, pp. 2–5, 2012.

[34] P. Sun, M. M. Hayat, and A. K. Das, "Bit error rates for ultrafast APD based optical receivers: Exact and large deviation based asymptotic approaches," *IEEE Trans. Commun.*, vol. 57, no. 9, pp. 2763–2770, Sep. 2009.

[35] P. Sun, M. M. Hayat, B. E. A. Saleh, and M. C. Teich, "Statistical correlation of gain and buildup time in APDs and its effects on receiver performance," *J. Lightw. Technol.*, vol. 24, no. 2, pp. 755–767, Feb. 2006.

[36] G. Kahraman, B. E. a Saleh, W. L. Sargeant, and M. C. Teich, "Time and frequency response of avalanche photodiodes with arbitrary structure," *IEEE Trans. Electron Devices*, vol. 39, no. 3, pp. 553–560, Mar. 1992.

[37] C. W. Helstrom, "Performance analysis of optical receivers by the saddlepoint approximation," *IEEE Trans. Commun.*, vol. COM-27, no. 1, pp. 186–191, Jan. 1979.
[38] M. G. Oberg and N. A. Olsson, "Crosstalk between intensity-modulated wavelength-division multiplexed signals in a semiconductor laser amplifier," *IEEE J. Quantum Electron.*, vol. 24, no. 1, pp. 52–59, Jan. 1988.
[39] R. Ramaswami and P. A. Humblet, "Amplifier induced crosstalk in multichannel optical networks," *J. Lightw. Technol.*, vol. 8, no. 12, pp. 1882–1896, Dec. 1990.
[40] K. Inoue, "Crosstalk and its power penalty in multichannel transmission due to gain saturation in a semiconductor laser amplifier," *J. Lightw. Technol.*, vol. 7, no. 7, pp. 1118–1124, Jul. 1989.
[41] G. P. Agrawal and N. A. Olsson, "Self-phase modulation and spectral broadening of optical pulses in semiconductor laser amplifiers," *IEEE J. Quantum Electron.*, vol. 25, no. 11, pp. 2297–2306, Nov. 1989.
[42] X. Wei and L. Zhang, "Analysis of the phase noise in saturated SOAs for DPSK applications," *IEEE J. Quantum Electron.*, vol. 41, no. 4, pp. 554–561, Apr. 2005.
[43] S. Xu, J. B. Khurgin, I. Vurgaftman, and J. R. Meyer, "Reducing crosstalk and signal distortion in wavelength-division multiplexing by increasing carrier lifetimes in semiconductor optical amplifiers," *J. Lightw. Technol.*, vol. 21, no. 6, pp. 1474–1485, Jun. 2003.
[44] M. Yoshino and K. Inoue, "Improvement of saturation output power in a semiconductor laser amplifier through pumping light injection," *IEEE Photon. Technol. Lett.*, vol. 8, no. 1, pp. 58–59, Jan. 1996.
[45] K. Sato, S. Kuwahara, and Y. Miyamoto, "Chirp characteristics of 40-gb/s directly modulated distributed-feedback laser diodes," *J. Lightw. Technol.*, vol. 23, no. 11, pp. 3790–3797, Nov. 2005.
[46] F. Koyama and K. Iga, "Frequency chirping in external modulators," *J. Lightw.Technol.*, vol. 6, no. 1, pp. 87–93, Jan. 1988.
[47] E. Peral, A. Yariv, and L. Fellow, "Large-signal theory of the effect of dispersive propagation on the intensity modulation response of semiconductor lasers," *J. Lightw. Technol.*, vol. 18, no. 1, pp. 84–89, Jan. 2000.
[48] A. E. Willner and W. Shieh, "Optimal spectral and power parameters for all-optical wavelength shifting: Single stage, fanout, and cascadability," *J. Lightw. Technol.*, vol. 13, no. 5, pp. 771–781, May 1995.
[49] D. Fitsios *et al.*, "High-gain 1.3 μm GaInNAs semiconductor optical amplifier with enhanced temperature stability for all-optical signal processing at 10 Gb/s," *Appl. Opt.*, vol. 54, no. 1, pp. 46–52, 2015.
[50] J. Hashimoto *et al.*, "1.3 um travelling-wave GaInNAs semiconductor optical amplifier," in *Proc. Conf. Opt. Amplifiers Their Appl.*, pp. 1–3, 2003.
[51] S. Tanaka, A. Uetake, S. Okumura, M. Ekawa, G. Nakagawa, and K. Morito, "Uncooled, polarization-insensitive AlGalnAs MQW-SOA module operable up to 75 °C with constant current," in *Proc. 37th Eur. Conf. Exhib. Opt. Commun.*, 2011, pp. 1–3.
[52] H. Wang *et al.*, "Temperature independent optical amplification in uncooled quantum dot optical amplifiers," in *Proc. Conf. Opt. Fiber Commun./Nat. Fiber Opt. Eng. Conf.*, 2008, pp. 1–3.
[53] Kamelian, "SOA pre-amplifier 1300 nm," [Online]. Available: http://www.kamelian.com/data/oa_13_ds.pdf, 2015.

Jose Krause Perin received the B.S. degree in electrical engineering from the Universidade Federal do Espirito Santo, Goiabeiras, Brazil, in 2013 and the M.S. degree in electrical engineering from Stanford University, Stanford, CA, USA, in 2015 where he is currently working toward the Ph.D. degree in electrical engineering.

His current research interests include optical-fiber communications, optical networks, digital signal processing, and digital communications.

Milad Sharif received the M.S. and Ph.D. degrees in electrical engineering from Stanford University, Stanford, CA, USA, in 2012. His current research interests include optical interconnects for data centers, optical circuit switching, and data center networking.

Joseph M. Kahn (M'90–SM'98–F'00) received the A.B., M.A., and Ph.D. degrees in physics from The University of California (U.C.), Berkeley, CA, USA, in 1981, 1983, and 1986, respectively.

From 1987 to 1990, he was at AT&T Bell Laboratories, Crawford Hill Laboratory, Holmdel, NJ, USA. He demonstrated multiGbit/s coherent optical fiber transmission systems and setting world records for receiver sensitivity. From 1990 to 2003, he was the Faculty in the Department of Electrical Engineering and Computer Sciences, U.C. Berkeley, performing the research on optical and wireless communications. Since 2003, he has been a Professor of electrical engineering at Stanford University, Stanford, CA, USA, where he heads the Optical Communications Group. His current research interests include fiber-based imaging, spatial multiplexing, rate-adaptive and spectrally efficient modulation and coding methods, coherent detection and associated digital signal processing algorithms, digital compensation of fiber nonlinearity, and free-space systems. In 2000, he helped found StrataLight Communications, where he served as the Chief Scientist from 2000 to 2003. StrataLight was acquired by Opnext, Inc., in 2009.

Prof. Kahn received the National Science Foundation Presidential Young Investigator Award in 1991. From 1993 to 2000, he served as a Technical Editor of IEEE PERSONAL COMMUNICATIONS MAGAZINE. Since 2009, he has been an Associate Editor of IEEE/OSA *Journal of Optical Communications and Networking*.